# Secondary Grouting Pressure Limit of Shield Tunnels in Loess Strata Based on Bolt Shear Behavior

Haolan Feng[1], Fei Ye[1*], Xiaobao Wen[1], Xingbo Han[1], Xing Liang[1], Pengfei Lei[1]

[1] School of Highway, Chang'an University, Nan Er Huan Zhong Duan, 710064 Xi'an, Shaanxi, China
* Corresponding author, e-mail: xianyefei@chd.edu.cn

**Abstract**

A loess stratum was selected as the research object, assuming that the slurry diffuses in a hemispherical shape during secondary grouting. Based on the unified strength theory describing the failure characteristics of loess and the critical condition of bolt shear failure, the critical pressure value of the secondary grouting in loess strata was determined theoretically. The reliability of the theoretical analysis was verified by the numerical modeling realizing the large deformation of formation and the dynamic injection of slurry. The critical grouting pressure of 821.80 kPa of theoretical calculation was obtained. Comparing the results of the numerical simulation analysis, it was found that the critical grouting pressure calculated using the theoretical equation had a safety index of 1.14. Bounded by $\beta_u$ (the ratio of expansion radius $R_p$ of soil plastic zone to the expansion radius $R_u$ of the slurry) equal to 2.65, the water pressure at the grouting port is the main factor affecting the upper limit of critical grouting pressure when it is less than 2.65, and the effective internal friction angle of soil layer is the main factor when it is greater than 2.65. The influence of matric suction on the upper limit of the critical grouting pressure can be ignored.

**Keywords**

loess stratum, shield tunnel, backfill grouting, bolt stress, critical pressure

## 1 Introduction

The total area of loess around the world is approximately 13 million square kilometers, and the area of the Loess Plateau in Shaanxi, Gansu, and Shanxi provinces in China exceeds 300,000 km². With the acceleration of urbanization in China, western cities, such as Xi'an, Lanzhou, and Taiyuan, are flourishing. As the most efficient infrastructure for alleviating urban traffic pressure, the metro needs to be urgently constructed. The shield method [1–3] is gradually being widely used because of its fast construction, minor disturbance to the stratum, and low labor intensity.

In the shield construction process, owing to the existence of shield tail clearance, the soil disturbance due to shield tunneling further increases. As an essential process during the construction of a shield tunnel, synchronous grouting can fill the gap in the shield tail in time and reduce the adverse impact of soil disturbance. When the effect of synchronous grouting on ground settlement control is poor, secondary grouting is needed. Secondary grouting is a grouting method that cement slurry and water glass are injected into the strata around the segment for

secondary sealing by using grouting holes on the segment. It has the advantages of adjustable construction parameters and large construction freedom, and is of great significance for dealing with construction problems such as surface deformation, segment dislocation and groundwater leakage. However, improper control of the secondary grouting parameters can easily cause engineering problems such as ground settlement overruns, segment ruptures, and bolt shear. Therefore, controlling the grouting pressure according to the stratum conditions during construction is an essential issue of concern to the industry.

However, the current research does not distinguish between synchronous grouting and secondary grouting but is uniformly referred to as backfill grouting. To solve the related problem of backfill grouting (including synchronous grouting and secondary grouting), Ye et al. [4, 5] assumed that the grouting slurry was viscosity time-varying, the slurry diffused along the hemisphere, the columnar [6] and the uniform cylindrical [7], and obtained the diffusion radius of the slurry and the pressure calculation

formula. Furthermore, Gou et al. [8] and Ye et al. [9] derived a circumferential distribution model of synchronous grouting filling pressures along the shield tail gap under the conditions of Bingham and Newton fluids. In addition, Liu et al. [10] proposed a diffusion analysis model of backfill grouting based on a Bingham fluid and found that the radial expansion distance of backfill grouting was proportional to the diversion capacity and initial grouting pressure, but inversely proportional to the yield stress of backfill grouting. Li [11] deduced the relationship between the surface settlement and theoretical grouting volume based on the heterogeneous distribution model of a loose foundation. Based on the shield tail grouting test, Liu et al. [12] analyzed the backfill grouting effect under different coatings. In terms of grouting application, Mei et al. [13] studied the settlement control effect of operating grouting on the upper railway through field tests and numerical simulation. Ding et al. [14] analyzed ground deformation induced by shield tunneling considering the effects of grouting.

Overall, although the theoretical research on the diffusion mechanism of backfill grouting has been more in-depth [15], owing to the adaptability of slurry and stratum, the engineering practicability and generalization of various slurry diffusion models still have certain limitations. Most of the existing numerical simulation methods ignore the fluid characteristics of the slurry and the large deformation characteristics of the soil. Therefore, the study of backfill grouting pressure (especially secondary grouting) for a specific stratum is the main task for future studies on backfill grouting.

Because the SPH (smoothed particle hydrodynamics) theory does not have a fixed grid, it has strong adaptability to problems such as fluid dynamics and large structural deformations. The theory is used to analyze engineering problems such as ground displacement caused by hydraulic jets [16], the flow of fresh concrete [17] and pile-soil interaction [18]. Li et al. [19] introduced the SPH method into the numerical simulation of synchronous grouting in a shield tunnel [20] and analyzed the diffusion mechanism and related parameters of synchronous grouting slurry during shield tunneling, as well as the large deformation characteristics and dynamic response of the soil and grouting body [21]. On this basis, Li et al. [19] used visual large-scale model tests to reproduce the real-time flow process of slurry in an irregular space and verified the rationality of the numerical simulation [22]. However, no scholars have applied this theory to study the secondary grouting process of shield tunnels.

In this work, based on a shield tunnel in the Xi'an metro, combined with theoretical analysis and numerical calculation methods, the upper limit pressure of the secondary grouting of a shield tunnel in a loess stratum was studied. Cities in loess areas, such as Xi'an, Lanzhou, and Taiyuan in western China, still have a great demand for metro traffic and water pipelines. Therefore, this study's theoretical results pertaining to the grouting pressure in a loess stratum are expected to be significantly helpful and provide guidance for field construction.

## 2 Theoretical analysis of grouting pressure in loess strata
## 2.1 Fundamental assumption
Loess exhibits the characteristics of being typically homogeneous, non-layered, and porous [23]; hence, it basically conforms to the precondition of continuous and uniform isotropy. Furthermore, the elastic-plastic analysis of hemispherical expansion in unsaturated loess strata was carried out based on the following assumptions. The schematic of the hemispherical expansion grouting model is shown in Fig. 1.

(1) Ignoring the permeability of the interface between the grout and soil, it is assumed that the backfill grouting first produces a compaction effect on the surroundings; if the grouting pressure is too large, the surrounding soil will split.

(2) Because the radius of the shield tunnel is much larger than the expansion range of the grouting slurry, the arc effect of the shield segment is ignored, and the outer wall of the segment is considered to be a plane.

(3) Considering synchronous grout and loess, as a whole, the stress-strain relationship obeys Hooke's law in the elastic region of the soil. The stress-strain relationship of the soil in the plastic zone obeys the unified strength criterion.
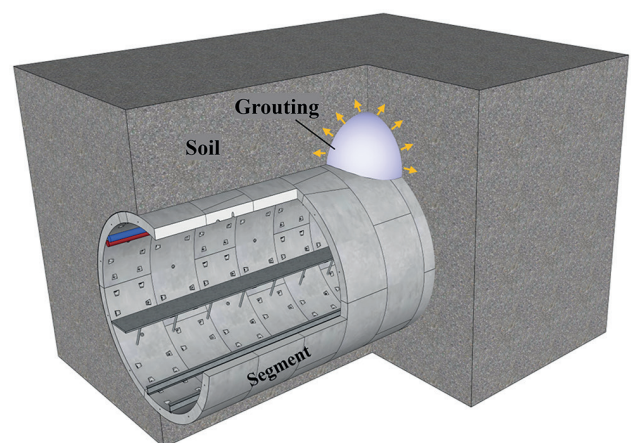


**Fig. 1** Schematic of the hemispherical expansion grouting model [6]

(4) The static earth pressure at an infinite distance and the internal pressure of the soil under the initial state are $P_0$, and the values in each direction are equal.

## 2.2 Elastic-plastic analysis

Supposing that the initial radius of the hemispherical slurry is $R_0$, the present radius in the expansion process is $R$, the corresponding elastic-plastic interface radius is $R_P$, and the soil outside $R_P$ remains elastic, the stress region of the hemispheric expansion of the grout is as shown in Fig. 2.

In unsaturated loess strata, the stress in the soil can be expressed by effective stress. In this study, the effective stress based on the suction stress was adopted, and the distribution of the matric suction in unsaturated soil was constant under drainage conditions. According to the elastic-plastic theory, the equilibrium equation of the spherical symmetry problem is:

$$\frac{d\tilde{\sigma}_r}{dr} + 2\frac{\tilde{\sigma}_r - \tilde{\sigma}_\theta}{r} = 0 .$$ (1)

In the above equation, $\tilde{\sigma}_r$ and $\tilde{\sigma}_\theta$ are the effective radial stress and the effective circumferential stress based on the suction stress, respectively.

The geometrical equation is:

$$\varepsilon_r = -\frac{du_r}{dr}, \varepsilon_\theta = -\frac{u_r}{dr} .$$ (2)

The elastic physical equation is:

$$\left.\begin{array}{l} \varepsilon_r = \dfrac{\sigma_r - 2v\sigma_\theta}{E} \\[2ex] \varepsilon_\theta = \dfrac{(1-v)\sigma_\theta - v\sigma_r}{E} \end{array}\right\},$$ (3)

where, $\varepsilon_r$ and $\varepsilon_\theta$ are the radial strain and circumferential strain, respectively; $u_r$ is the radial displacement of the soil, $E$ is the elastic modulus of soil, and $v$ is the Poisson ratio of soil.

The boundary conditions are:

$$\left.\begin{array}{l} \tilde{\sigma}_r|_{r=R_u} = P \\[1ex] \lim_{r\to\infty}\sigma_r = P_0 \end{array}\right\},$$ (4)

where, $P$ is the grouting pressure, and $P_0$ is the groundwater pressure at the grouting hole.

For the study of the yield criterion of unsaturated loess, Zhang et al. [24] assumed that when the two large shear stresses and normal stress influence the functions of the double shear unit of unsaturated soil to reach a certain limit,
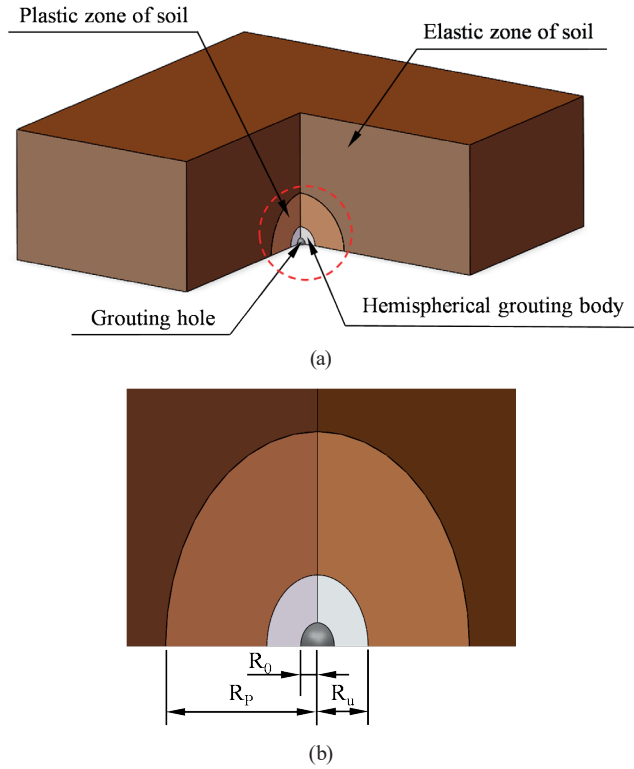


(a)



(b)

**Fig. 2** Stress region and radius indication under hemispherical grouting a) stress region indication, b) model-related radius

the unit begins to yield failure. To accurately describe the properties of unsaturated loess, assuming that the pressure is positive, the unified yield criterion of unsaturated loess is expressed by Eq. (5):

$$\begin{array}{l} \tilde{\sigma}_r = M'\tilde{\sigma}_\theta + \sigma'_0, \\[2ex] M' = \dfrac{2(1+b)(1+\sin\varphi') + mb(\sin\varphi' - 1)}{[2(1+b) - mb](1-\sin\varphi')}, \\[2ex] \sigma'_0 = \dfrac{4(1+b)c''\cos\varphi'}{[2(1+b) - mb](1-\sin\varphi')}, \end{array}$$ (5)

where, $\tilde{\sigma}_r$ and $\tilde{\sigma}_\theta$ are the effective radial and effective circumferential stresses, respectively. $M'$ and $\sigma_0'$ are the unified strength criterion parameters for unsaturated loess; $m$ is an intermediate principal stress parameter; and $b$ is a unified strength criterion parameter. When $b = 0$, the strength criterion is the M-C strength criterion, and when $b = 1$ is used, the strength criterion is the double shear stress strength criterion. The internal friction angle is the effective friction angle $\varphi'$ and the cohesion is $c'' = c' + c_s$. $c'$ is the cohesion of the unsaturated undisturbed soil and $c_s$ is the suction stress. Ye et al. [25] assumed that the stress-strain relationship in the plastic zone obeys the M-C strength criterion when studying the critical grouting pressure of shield tunnels in clay strata.

Regarding the shear strength of unsaturated undisturbed loess, Yuan et al. [26] and Bi et al. [27] studied the shear strength of unsaturated undisturbed loess based on suction stress, as follows:

$$\tau_f = \sigma' \tan\varphi' = (\sigma - u_a - c_s)\tan\varphi',$$
$$c_s = -\frac{u_a - u_w}{\left[1 + \left(\alpha(u_a - u_w)^n\right)\right]^{1-1/n}}, \tag{6}$$

where, $\varphi'$ is the effective internal friction angle, and $\alpha$ and $n$ are the fitting parameters of the soil-water characteristic curve (SWCC). It was found that the Van Genuchten model is more suitable for SWCC [27], so the parameter $c_s$ of suction stress in this study was taken from the Van Genuchten model. That is, $\alpha = 6.43$ kPa, $n = 1.93$ and $m = 0.33$. Additionally, Wang [28] conducted numerous experiments on unsaturated undisturbed loess in eastern Gansu. Based on the power function relationship between the matric suction and cohesion of unsaturated undisturbed loess combined with SWCC fitting, the cohesion of the unsaturated undisturbed loess is $c' = 13.14 + 2.349(u_a - u_w)^{0.541}$.

In the field grouting process, with an increase in the grouting pressure, the soil at the edge of the slurry gradually enters the yield state. The critical pressure of the soil entering the plastic state from Eqs. (1)–(5) is

$$P_P = P_0 + \frac{2\left[\sigma'_0 + (M'-1)P_0\right]}{2 + M'}. \tag{7}$$

Further, the stress and displacement of the elastic region $(r \geq R_P)$ are obtained.

$$\left.\begin{aligned}
\tilde{\sigma}_r &= P_0 + (P_P - P_0)\left(\frac{R_P}{r}\right)^3 \\
\tilde{\sigma}_\theta &= P_0 - \frac{P_P - P_0}{2}\left(\frac{R_P}{r}\right)^3 \\
u_r &= \frac{2v-1}{E}P_0 r + \frac{(1+v)(P_P - P_0)r}{2E}\left(\frac{R_P}{r}\right)^3
\end{aligned}\right\} \tag{8}$$

The stress of the plastic zone $(R_u \leq r \leq R_P)$ is:

$$\left.\begin{aligned}
\tilde{\sigma}_r &= -\frac{\sigma'_0}{M'-1} + C_1 r^{\frac{2(M'-1)}{M'}} \\
\tilde{\sigma}_\theta &= -\frac{\sigma'_0}{M'-1} + \frac{C_1}{M'}r^{\frac{2(M'-1)}{M'}}
\end{aligned}\right\} \tag{9}$$

At the elastoplastic interface $(r = R_P)$, its effective radial stress is the critical expansion pressure $P_P$, that is,

$$\tilde{\sigma}_r \big|_{r=R_p} = P_P. \tag{10}$$

Substituting Eq. (10) into Eq. (9), the following is obtained:

$$C_1 = R_P^{\frac{2(M'-1)}{M'}}\left(P_P + \frac{\sigma'_0}{M'-1}\right). \tag{11}$$

By substituting the boundary condition $\sigma_r = \big|_{r=R_u} = P$ into Eq. (9), the relationship between the plastic zone radius $R_u$, current slurry radius $R_u$, and pressure level $F$ can be obtained as follows:

$$\beta = \frac{R_P}{R_u} = \left[\frac{(M'-1)P+\sigma'_0}{(M'-1)P_P+\sigma'_0}\right]^{\frac{M'}{2(M'-1)}} = F^{\frac{M'}{2(M'-1)}}, \tag{12}$$

$$F = \frac{(M'-1)P+\sigma'_0}{(M'-1)P_P+\sigma'_0}. \tag{13}$$

In Eq. (12), $\beta$ is the ratio of the expansion radius $R_P$ of the plastic zone to the expansion radius $R_u$ of the slurry in the unsaturated undisturbed loess.

The relationship between the initial radius of the slurry $R_0$ and the present radius $R_u$ is obtained.

$$\begin{aligned}
\frac{1}{\xi} = \frac{R_0}{R_u} &= \frac{(1-2v)(M'+1)}{E(M'+2)}\left(P_P + \frac{\sigma'_0}{M'-1}\right)\left(\beta^{\frac{2(M'-1)}{M'}} - \beta^3\right) \\
&+ \frac{\sigma'_0(1-2v)}{E(M'-1)}(\beta^3 - 1) - \delta\beta^3 + 1
\end{aligned} \tag{14}$$

In Eq. (14), $\delta = \frac{2v-1}{E}P_0 + \frac{(1+v)(P_P - P_0)}{2E}$, $\xi$ is the slurry expansion rate.

## 2.3 Critical grouting pressure

In the field grouting process, the grouting pressure is too high, which may lead to slurry split soil and an increase in the segment stress, resulting in bolt and segment joint concrete damage and bolt shear failure. When the grouting pressure increases to a certain extent, the pressure generated by the slurry on the segments causes the connection bolt to bear excessive shear stress, which makes it easy to cut the bolt. Therefore, in this study, the critical value of the grouting pressure was deduced by analyzing the shear failure of the segment connection bolts. The shearing effect of bolts is shown in Fig. 3.

The pressure on the segments during slurry compaction is:

$$F_g = P\pi R_u^2 = \pi P R_u^2. \tag{15}$$

The pressure of plastic soil on the segments is:

$$F_P = \int_{R_u}^{R_P} \tilde{\sigma}_\theta 2\pi r \, dr = \pi\left[-\frac{\sigma'_0}{M'-1}\left(R_P^2 - R_u^2\right) + C_1\left(R_P^{2/M'} - R_u^{2/M'}\right)\right]. \tag{16}$$
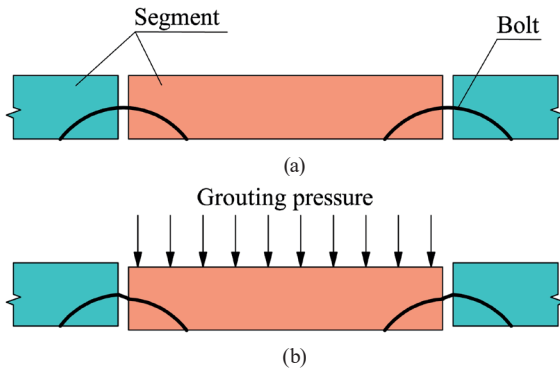
**Fig. 3** Shearing effect of bolts a) normal segment, b) segment misaligned by grouting pressure

The total pressure of compaction grouting on the segments is:

$$F_s = F_g + F_P = \pi \left[ PR_u^2 - \frac{\sigma_0'}{M'-1}\left(R_P^2 - R_u^2\right) + C_1\left(R_P^{2/M'} - R_u^{2/M'}\right) \right]. \quad (17)$$

When the grouting pressure on the segments is concentrated at the back of individual segments, there is a trend of dislocation between the stressed segment and its adjacent segment. When the load reaches a certain degree, dislocations may occur between the segments or even cut the connection bolt. The maximum shear stress on the bolts [29] is calculated as follows:

$$\tau_{max} = \frac{l_b - \lambda}{\pi r_b^2 l_b} Q = \frac{l_b - \lambda}{\pi r_b^2 l_b} \cdot \frac{F_s}{N_i},$$

where, $l_b$ is the effective length of the bolt, $Q$ is the equivalent shear force of the bolt, $\lambda$ is the length between the two shear contact points of the bolt, and $r_b$ is the bolt radius.

Combined with the pressure Eq. (17) produced by grouting on the segments, the shear force on the bolt is.

$$\tau_{max} = \frac{l_b - \lambda}{\pi r_b^2 l_b} \frac{F_S}{N_i}$$

$$= \frac{\left(l_b - \lambda\right)\left[ PR_u^2 - \dfrac{\sigma_0'}{M'-1}\left(R_P^2 - R_u^2\right) + \left(R_P^{2/M'} - R_P^{2/M'}\right) \right]}{r_b^2 l_b N_i} \quad (18)$$

Eqs. (12) and (13) are substituted into Eq. (18) and simplified to

$$\frac{1}{R_u^2} = \left[ \frac{\sigma_0'}{M'-1}\beta^{\frac{2(M'-1)}{M'}} + P_P\beta^2 \right] \frac{\left(l_b - \lambda\right)}{r_b^2 l_b N_i \tau_{max}}. \quad (19)$$

By substituting Eq. (19) into Eq. (14), the equation for $\beta$ becomes

$$\left(M - N - \delta\right)\beta^3 + \left(N - \frac{\sigma_0'}{M'-1}W\right)\beta^{\frac{2(M'-1)}{M'}} - P_P W\beta^2 - M + 1 = 0 \quad (20)$$

In the formal, $M = \dfrac{\sigma_0'(1-2v)}{E(M'-1)}$, $N = \dfrac{(1-2v)(M'+1)}{E(M'+2)}\left(P_P + \dfrac{\sigma_0'}{M'-1}\right)$, $W = \dfrac{R_0\left(l_b - \lambda\right)}{r_b^2 l_b N_i \tau_{max}}$, $P_P = P_0 + \dfrac{2\left[\sigma_0' + (M'-1)P_0\right]}{2 + M'}$.

By substituting the allowable shear stress of the bolt into Eq. (20), the ratio $\beta_u$ of the expansion radius of the soil plastic zone to the expansion radius of the slurry is solved by considering the shear failure of the bolt. Substituting $\beta_u$ into Eqs. (12) and (13), and replacing $P$ with $P_{u2}$, the formula for the critical value of $P_{max}$ for the grouting pressure considering bolt shear failure is

$$P_{max} = P_{u2} = \left( \frac{2\sigma_0' + 3M'P_0}{2 + M'} + \frac{\sigma_0'}{M'-1} \right)\beta_u^{\frac{2(M'-1)}{M'}} - \frac{\sigma_0'}{M'-1}. \quad (21)$$

**2.4 Engineering application**

Based on an interval shield tunnel of the Xi'an Metro, the vault depth of the interval tunnel is approximately 11.4–19 m, and the upper strata are mainly $Q_3$ and $Q_2$ old loess strata. The shield tunnel passes mainly through the $Q_2$ old loess stratum. The corresponding physical and mechanical parameters of the strata are presented in Table 1. The groundwater pressure $P_0$ at the grouting point is 50 kPa, and the grouting hole radius $R$ is 2.5 cm.

The lining segments adopt reinforced concrete segments with a 1500 mm ring width. The inner and outer diameters of the segment are 5400 and 6000 mm, respectively. The thickness is 300 mm, the strength grade is C50, and the impermeability grade is P12. The segment is circularly divided into six blocks, and the F block is inserted longitudinally. The longitudinal and circumferential hand holes of the segment are connected using M27 bending bolts, with a performance grade of 8.8. The bolt material is low-carbon alloy steel, allowable shear stress $|\tau|$ is 60 MPa, and minimum yield strength is 640 MPa [30]. There are two bolts around each joint, making it a total of 12; with ten bolts bring arranged longitudinally (2 each except the key block). The bolt length $l_b$ of the shield tunnel in this interval

**Table 1** Physical and mechanical parameters of the strata in the study area

| Soil layer | Matric suction (kPa) | Cohesive force (kPa) | Effective friction angle (°) | Elastic modulus (kPa) | Gravity (kN/m³) | Poisson ratio |
|---|---|---|---|---|---|---|
| $Q_3$ Neo-loess | 73 | 37.0 | 22.5 | 3000 | 15.3 | 0.3 |
| $Q_2$ Old loess | 67 | 36.0 | 22.5 | 3000 kPa | 16.9 | 0.3 |

is 0.4 m, the length $\lambda$ between the two shear contact points of the bolt is 0.01 m, and the bolt radius $r_b$ is 0.015 m. The number $N$ of connecting bolts near the grouting hole of the standard block and adjacent block is 8.

Substituting $P_0$ = 50 kPa, $s$ = 67 kPa, $\alpha$ = 6.43 kPa, $n$ = 1.93, $b$ = 0, $m$ = 0.33 and $\varphi'$ = 22.5° into Eq. (6), $c''$ = 35.98 kPa and $P_P$ = 129.72 kPa can be obtained.

The ratio $\beta_u$ of the expansion radius $R_P$ of the plastic zone to the expansion radius $R_u$ of the slurry is 3.6587, obtained by substituting the allowable shear stress into Eq. (20). $P_{max}$ = 821.80 kPa was obtained by substituting $E$ = 3000 kPa, $v$ = 0.3 and $P_P$ = 129.72 kPa into Eq. (21).

## 3 Grouting analysis based on the SPH theory

Based on the theoretical analysis of the critical grouting pressure in the loess stratum and the SPH theory, this section simulated the secondary grouting process of loess shield tunnels. At first, the SPH was used to simulate non-axisymmetric problems in astrophysics [31]. With an understanding of the ability of the SPH algorithm to deal with complex physical problems, its application range is also becoming increasingly extensive. As a Lagrange method, the SPH retains the properties of the macroscopic equations of continuum mechanics and has partial properties of molecular dynamics [32]. The basic idea of the SPH method is to describe the continuum (or solid) with an interacting particle group, where each particle carries physical quantities such as mass and velocity. The mechanical behavior of the entire system is obtained by solving the dynamic equation of the particle group and tracking the motion trajectory of each particle.

Because the SPH has the advantage of no fixed grid, it has strong adaptability to fluid power and large deformation of the structure. In this study, finite element software was used to define the traditional continuous element. During the analysis of the grouting process, a threshold was set to convert the element mesh into particles.

## 3.1 Establishment of the grouting model

In the process of numerical analysis [33, 34], the strength criterion of loess is the selected M-C strength criterion;

that is, the unified strength criterion parameter $b$ is 0. The basic parameters of the soil layers are listed in Table 1. The basic parameters of the segments, bolts, and synchronous grouting are shown in Tables 2 and 3 [35]. Because synchronous grouting basically reaches the initial setting state during secondary grouting, the synchronous grouting parameters take the corresponding parameters of the initial setting stage.

The gravity $\gamma$ of the segment concrete is 25 kN/m³, the elastic modulus $E$ is $2.648 \times 10^4$ MPa, and the Poisson's ratio $v$ is 0.167. The parameters required for the plastic damage model of concrete are as follows: a dilatancy angle of 15°, an eccentricity of 0.1, a ratio of biaxial to the uniaxial compressive strength of 1.16, and a yield constant of 0.6667.

The state equation $U_S - U_P$ was selected to describe the slurry characteristics when simulating the grouting process. The relevant parameters of $U_S - U_P$ are related to the characteristics of the material. According to the relevant research results [36], the volume velocity of the slurry, that is, the intercept $C_0$ of the curve is 2300 m/s, the coefficient $s$ of the slope of the curve is 1.5, and the Gruneisen coefficient $\gamma_0$ is 1. Simultaneously, to describe the deformation process of soil under grouting pressure using the large deformation characteristics of the SPH theory, the bolt stress changes in the grouting process were analyzed. When the strain of the grouting body and soil layer unit reaches a threshold of 0.001, it changes into particles. The overall model is shown in Fig. 4, and a section of the segment is shown in Fig. 5.

Besides, a model profile of segments and soil-slurry layers is shown in Fig. 6.

## 3.2 Initial stress analysis of the bolt

Bolt stress is related to many factors, such as ground stress, and the position of the key block and the grouting hole. Therefore, it is difficult to determine the critical grouting pressure of a specific stratum and the shield tunnel design parameters under complex conditions. In this study, the stress of the bolt was considered, and the stress of the bolt in the initial gravity field was analyzed.

Table 2 Basic parameters of the synchronous slurry

| Member | Gravity (kN/m³) | Elastic modulus (MPa) | Poisson ratio | Cohesive force (kN/m²) | The angle of internal friction (°) |
|---|---|---|---|---|---|
| Synchronous slurry | 20 | 150 | 0.22 | 100 | 36 |

Table 3 Basic parameters of bolts [35]

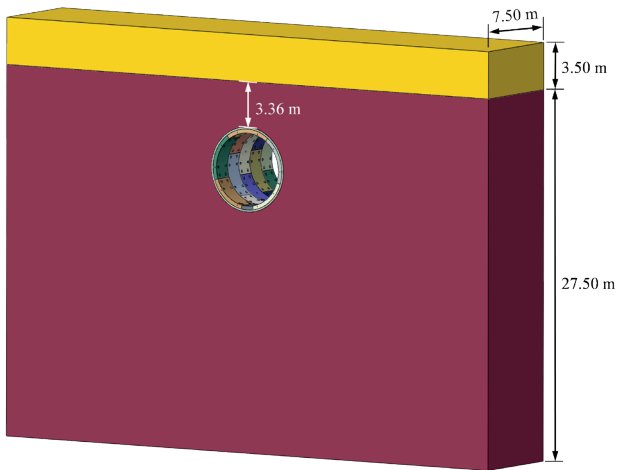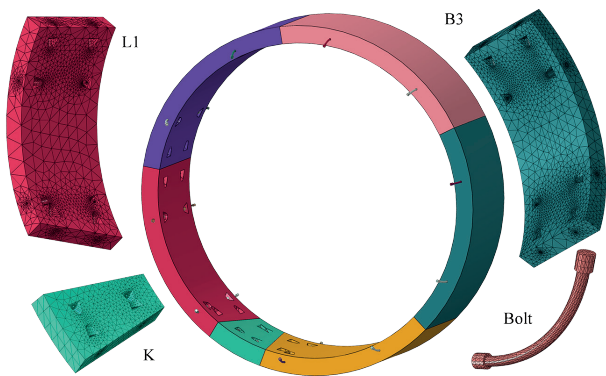| Member | Gravity (kN/m³) | Elastic modulus (MPa) | Poisson ratio | Yield strength (MPa) | Tensile strength (MPa) |
|---|---|---|---|---|---|
| Bolt | 78.5 | $2.1 \times 10^5$ | 0.29 | 640 | 800 |

**Fig. 4** Overall model



**Fig. 5** Cross section decomposition of the segment



**Fig. 6** Model profiles of segments and soil-slurry layers

The most unfavorable stress conditions on the bolt were obtained, and a grouting simulation was carried out to further study the influence of grouting on the bolt stress. However, because the segments and bolts on both sides are greatly affected by the boundary conditions, the stress of the bolts in the middle ring segment can best reflect the effect of grouting. Therefore, the stress of the bolts involved in the middle ring was analyzed.

By using the method of explicit dynamics, the gravity field of the shield tunnel project was solved, and the bolt stress of the key block at the upper, left, and lower points were analyzed. The distribution of segments under the three conditions is shown in Fig. 7.
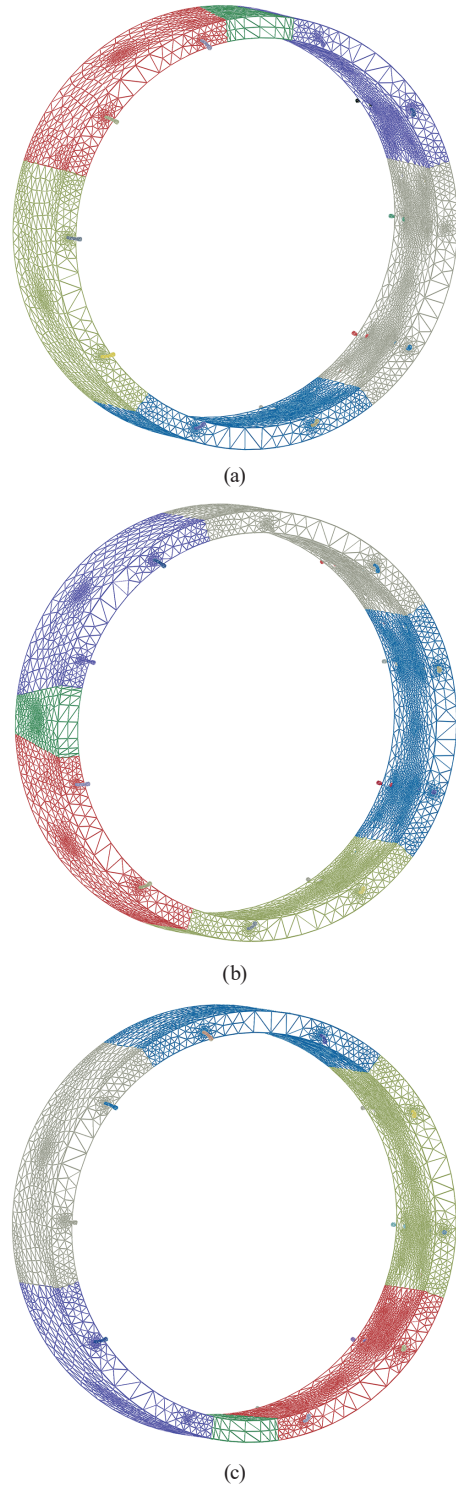


(a)



(b)



(c)

**Fig. 7** Segment grids corresponding to different positions of the key block a) the key block is located at 0°, b) the key block is located at 180°, c) the key block is located at 270°

The bolt stress for the three working conditions above under gravity was solved, and the position of each bolt was replaced by an angle. The circumferential and longitudinal bolt stresses corresponding to the three working conditions were then compared. The heading direction is defined as the front; that is, the large side of the key block is at the front. Stress comparisons of the circumferential and longitudinal bolts are shown in Figs. 8 and 9, respectively.

As shown in Fig. 8, the stress values of the circumferential bolts on both sides are not significantly different; however, the stress values of most bolts are greater than those of the front bolts. The circumferential bolt stress on the opposi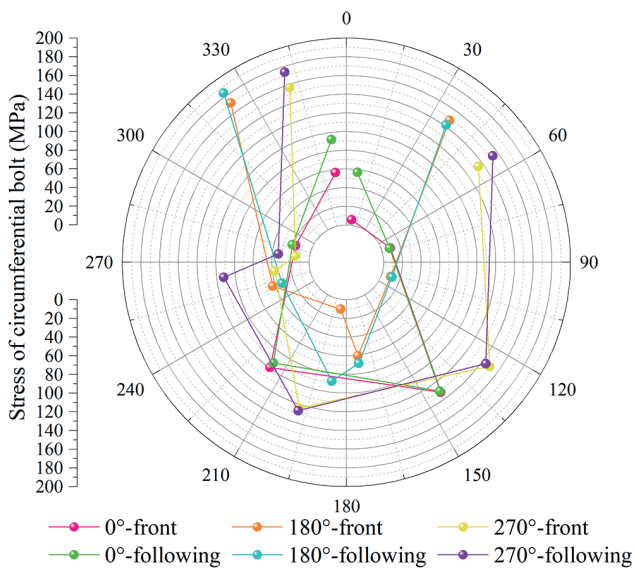te sides of the key block is the largest for the entire ring and does not change with the change in the position of the key block. Under the three working conditions, when the key block is located at 180°, the circumferential bolt stress adjacent to the standard block near 0° is the largest.

As shown in Fig. 9, the stress values of the longitudinal bolts on both sides are significantly different, and the stress value of the following bolt is significantly larger than that of the front bolt. The position of the maximum longitudinal bolt stress corresponds to the position of the top block; that is, the maximum longitudinal bolt stress is located at the adjacent block position near both sides of the key block. The longitudinal bolt position of the maximum stress is the adjacent block near the key block position.

In general, when the key block is located at 180°, the stress of the longitudinal bolt at this point is the largest, and the stress of the circumferential bolt at the 0° standard block on the opposite side is the largest. The stress on the longitudinal bolts is greater than that on the circumferential bolts. In other words, when the key block is located at 180°, it is considered to be a relatively unfavorable condition for the bolt under the initial stress. Therefore, this study analyzed the bolt stress corresponding to the secondary grouting process based on this unfavorable condition. Figs. 10 and 11 show the stresses of some circumferential bolts and longitudinal bolts when the key block is located at 180°, respectively.
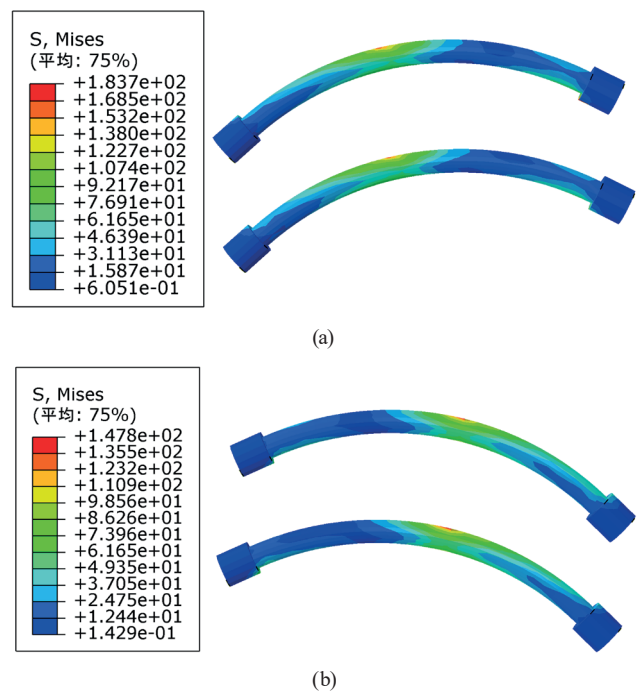


**Fig. 8** Stress comparison of circumferential bolts
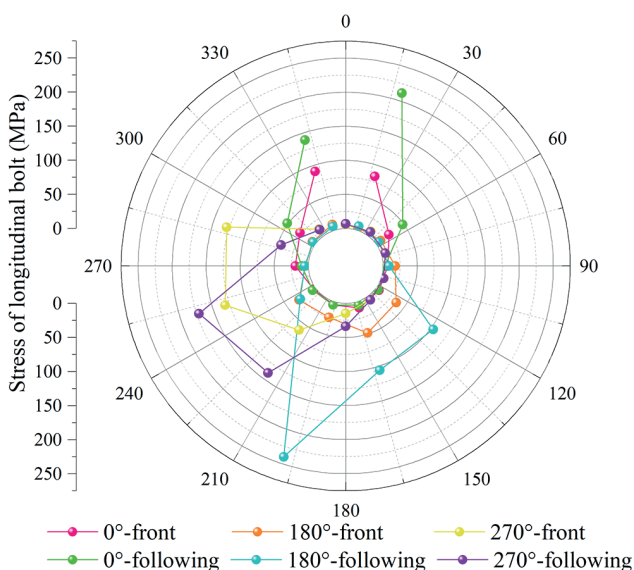


**Fig. 9** Stress comparison of longitudinal bolts



**Fig. 10** Stress of some circumferential bolts when the key block is located at 180° a) left side of the standard block A2, b) right side of the standard block A2
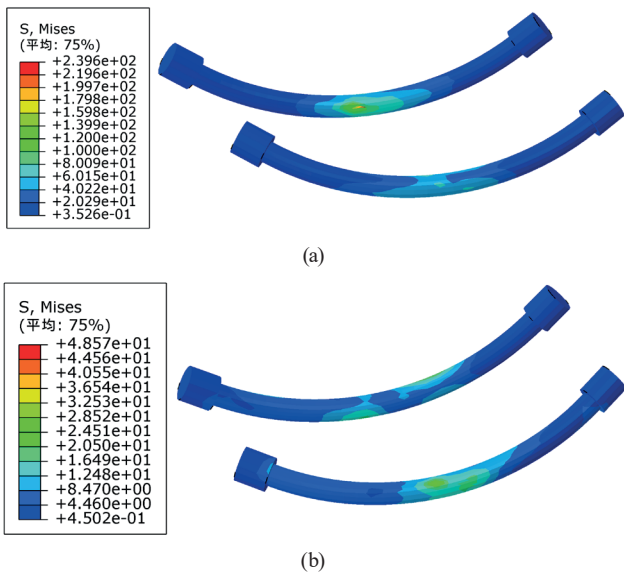
(a)



(b)

**Fig. 11** Stress of some longitudinal bolts when the key block is located at 180° a) left side of key block K, b) right side of key block K

By observing the stress cloud diagram of some circumferential and longitudinal bolts when the key block is located at 180°, it is found that the stress on the outer side of the circumferential bolt is larger than that on the inner side. As far as the stress of the longitudinal bolts is concerned, most of the longitudinal bolts have a larger stress on the outside than on the inside, but there is also a phenomenon of lateral stress concentration.

### 3.3 Bolt stress under grouting

The following points must be explained when introducing bolt stress under grouting. First, the SPH theory is used to analyze the stress of bolts under gravity conditions with significant errors and inaccurate analysis results. In the simulation of the grouting process, the grouting pipe is regarded as a rigid body, and the fixed rigid body affects the bolt stress under gravity. In addition, an explicit dynamic analysis cannot set the working conditions. Based on the analysis of bolt stress under the action of gravity in Section 3.2, the gravity analysis results cannot be set as the initial stress field of the grouting process because the continuous element cannot be transformed into particles under certain threshold conditions.

For these reasons, it is impossible to simulate the grouting process based on an analysis of the initial gravity stress. However, because the M27 bolt is made of low-carbon alloy steel, its material properties are in accordance with the condition of the stress linear superposition principle. Therefore, under the premise of analyzing the bolt stress under gravity in Section 3.2, the grouting process

under the most unfavorable segment assembly conditions was simulated. Considering that the contact area between the key block and the stratum is small, the corresponding stress area is also small. Moreover, there are only four corresponding circumferential bolts. Under the action of secondary grouting, the key block segment can be dislocated and damaged. Therefore, secondary grouting does not require the key block hoisting hole as the grouting point in field construction. Based on the above conditions and the analysis results in Section 3.2, this section simulates the grouting conditions when the key block is located at 180°, the 0° standard block hoisting hole is used as the secondary grouting hole, and analyses the stress conditions of the soil, segments, and bolts under the action of grouting. Considering that excessive displacement of the segment during secondary grouting may lead to the occurrence of segment rupture prior to bolt shear, combined with field construction experience, specified requirements [37] and monitoring data of tensile strength [38]. It is assumed that the segment reaches the failure state when the maximum displacement is greater than 3 cm.

Simultaneously, to reflect the advantages of the SPH theory in the analysis of the impact and large deformation problems, the critical grouting pressure of 821.8 kPa obtained from the study in Section 2.4 is used as the pressure of secondary grouting, and the grouting body is transformed from $t = 0$ to particles. At the same time, the units with interactions between the synchronous grouting layer, old loess, neo-loess, and secondary grouting body are set to transform into particles when the stress reaches a certain threshold. Fig. 12 shows the stress or displacement state of the synchronous slurry, soil, and segment under the action of secondary grouting.

The working condition of secondary grouting through the hoisting hole of a 0° standard block was simulated. According to the analysis results, when the segment displacement reaches approximately 3 cm, the bolt stress does not reach yield stress of 640 MPa. Therefore, the bolt stress under gravity conditions and the bolt stress when the segment displacement reaches 3 cm under grouting were superimposed. The corresponding bolt stresses under the grouting and after superposition are shown in Figs. 13 and 14, respectively.

In contrast to the bolt stress under gravity, the stress value of the circumferential bolt under grouting is larger than that of the longitudinal bolt. Additionally, the stress distribution of the circumferential bolt is the same as that of the bolt under gravity, and the maximum stress values
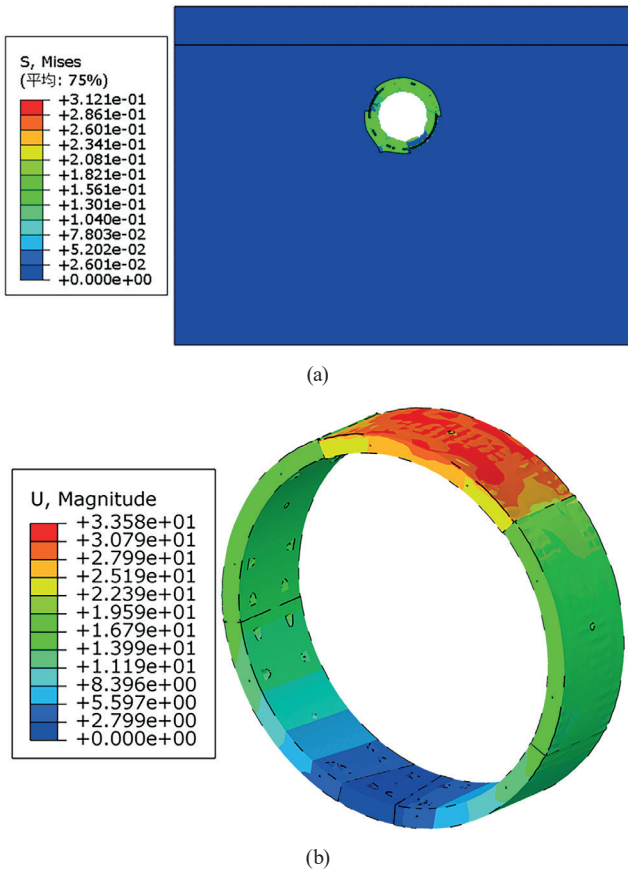
(a)



(b)

**Fig. 12** Structural stress and displacement under secondary grouting a) stress of soil and grouting, b) segment displacement



**Fig. 13** Bolt stress under secondary grouting



**Fig. 14** Linear superposition value of bolt stress under gravity and grouting

of the circumferential bolt are concentrated outside the bolt. Therefore, the superimposition of the bolt stress value under gravity and grouting has certain rationality. After superposition, the stress values of the circumferential bolts are still larger than those of the longitudinal bolts. The stress values of four circumferential bolts in the 0° standard block are 322.3 MPa, 560.5 MPa, 527.7 MPa and 410.6 MPa, respectively. The maximum stress of the bolt is 560.5 MPa, which is less than the yield stress (640 MPa) of the M27 bolt.

If the safety factor between the numerical simulation results and yield stress of the M27 bolt is $h$, then

$$S_{\max} \cdot h = \sigma_s . \tag{22}$$

Substituting $S_{\max} = 560.5$ MPa and $\sigma_s = 640$ MPa into Eq. (22), $h = 1.14$ is obtained. Therefore, the critical grouting pressure of 821.80 kPa obtained by the theoretical analysis has a certain safety limit, and the model has a guiding significance for shield tunnel construction in loess strata. It must be emphasized that the distribution of hydrostatic pressure varies greatly with strata. In other words, the water pressure $P_0$ at the grouting outlet (hydrostatic
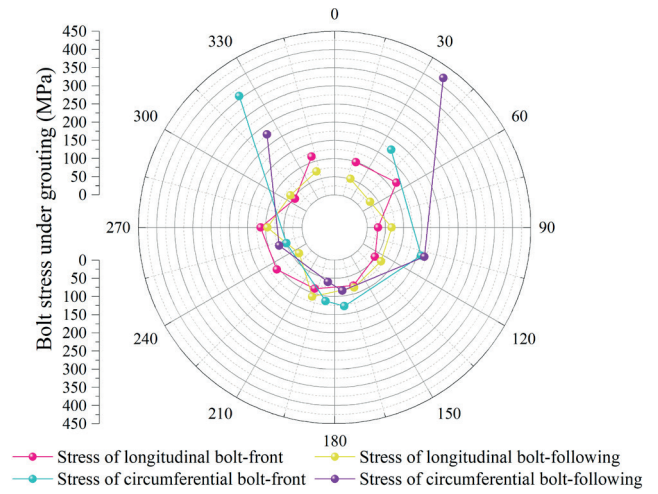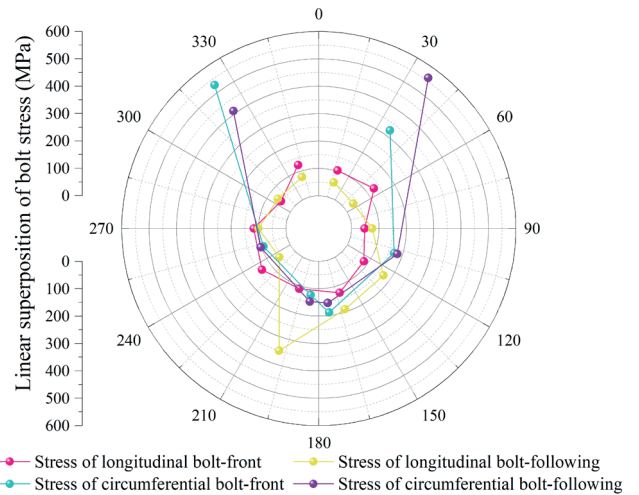
pressure) may be the same under different loess ground conditions and buried depths. Therefore, as far as the theoretical formula is concerned, it can be applied to the calculation of the secondary grouting pressure limit during the construction of shield tunnels in loess strata without considering the buried depth conditions of the urban tunnels.

## 4 Sensitivity analysis of the grouting pressure

The above content verifies the reliability of the theoretical analysis; therefore, this model can be used to solve the critical grouting pressure of shield tunnels in loess. Furthermore, a sensitivity analysis of the factors affecting the critical grouting pressure has important practical significance for determining the grouting pressure at construction sites. The theoretical formula of grouting pressure in loess strata in this study involves variable parameters, such as the unified strength criterion parameter $b$, water

pressure $P_0$ at the grouting outlet, effective internal friction angle $\varphi'$ of soil, and matric suction $s$. First, the influence of the uniform strength criterion parameter on the grouting pressure critical value was analyzed. Then, based on the Sobol method, a sensitivity analysis was conducted on the factors affecting the grouting pressure limit, such as the water pressure $P_0$ at the grouting outlet, effective internal friction angle $\varphi'$ of the soil, and matric suction $s$.

## 4.1 Unified strength criterion parameters

The unified strength criterion coefficient was set as 0/1. In Section 2, when calculating the grouting pressure in the loess stratum, it is assumed that the stress-strain relationship in the plastic zone obeys the M-C strength criterion, namely $b = 0$. This study analyses the grouting pressure of a loess stratum when the stress-strain relationship of the plastic zone obeys the double shear stress strength criterion ($b = 1$) and calculates the ratio of the expansion radius $R_P$ of the plastic zone to the expansion radius $R_u$ of slurry and the limit value of grouting pressure. The grouting pressures calculated based on the different strength criterion coefficients are listed in Table 4.

As shown in Table 4, compared to the M-C strength criterion ($b = 0$), when the double shear stress strength criterion ($b = 1$) is selected in the plastic zone, the ratio of the soil plastic zone to the expansion radius of the slurry decreases, but the limit value of the grouting pressure increases. This shows that when the double shear stress strength criterion is selected for the plastic zone, the soil plastic zone under grouting is smaller, but the grouting pressure is larger.

Specifically, the differences in the ratio of the soil plastic zone to the slurry expansion radius and the limit value of the grouting pressure obtained by the double shear stress strength criterion and the M-C strength criterion in the plastic zone are -0.0896 and 45.63, respectively; and the differential percentages of the relative error are 0.62 % and 1.35 %, respectively. It can be observed that when the grouting pressure of the shield tunnel in the loess stratum is determined, the selection of the strength criterion of the plastic zone has little effect on the calculation results. To simplify the calculation process, the strength criterion parameter $b$ was set to 0.

## 4.2 Limit value of grouting pressure

The sensitivity analyses performed include local sensitivity analysis (LSA) and global sensitivity analysis (GSA). Because the local sensitivity analysis method cannot evaluate the interaction between model parameters when the model parameters and structural response are nonlinear, the analysis results depend on the selection of fixed points, and the model parameters of different orders of magnitude cannot provide effective analysis results. In this study, the global sensitivity analysis method was selected to test the influence of simultaneous changes in multiple parameters on structural response. Based on the single-model parameter variation range as the whole definition domain, the sensitivity of a single model parameter is analyzed when all parameters change simultaneously.

Through the analysis of the relationship between the input variables and the output response of the model, the importance of the input variables was judged based on the sensitivity coefficient of each input variable, and the important and irrelevant variables were identified to realize the preliminary understanding and prediction of the model [39]. When determining grouting parameters in construction, input variables with large sensitivity coefficients can be considered to reduce construction costs. In the sensitivity analysis, the variation ranges of water pressure $P_0$ at the grouting outlet, effective internal friction angle $\varphi'$ of soil, and matric suction $s$ in loess strata were investigated. The variation ranges are (0, 500 kPa), (0, 35°), and (50, 300 kPa), respectively.

In the sensitivity analysis of the grouting pressure limit, the ratio $\beta_u$ of the soil plastic zone expansion radius $R_P$ to the slurry expansion radius $R_u$ should be obtained by solving the equation, after which the sensitivity analysis was carried out for a specific value $\beta_u$. According to the results, the $\beta_u$ does not exceed 5. To explore the influence of various factors on the grouting pressure limit, the numerical

**Table 4** Upper limit of the grouting pressure under different strength criterion parameters

| Strength criterion parameter | Ratio $\beta_u$ of soil plastic zone $R_P$ to slurry expansion radius $R_u$ | Limit value of grouting pressure (kPa) |
|---|---|---|
| 0 | 3.6587 | 821.80 |
| 1 | 3.5691 | 867.43 |
| Differentials | -0.0896 | 45.63 |
| Percentage of relative error (%) | 0.62 | 1.35 |

Notes: Differentials refer to $\beta_u$ or limit the value of grouting pressure ($b = 1$) minus the corresponding value ($b = 0$). Percentage of relative error refers to the absolute value of differentials divided by the average of the corresponding values (corresponding values when $b$ is equal to 0 and 1).

variation range of $\beta_u$ was set to (1, 8) when the sensitivity analysis of grouting pressure limit factors was performed. The variation trend of the sensitivity coefficient of the grouting pressure limit influencing factors with $\beta_u$ is shown in Fig. 15.

It can be seen from the figure that the matric suction has little effect on the grouting pressure limit. The influence conditions of the water pressure at the grouting outlet and the effective friction angle on the grouting pressure limit change when $\beta_u$ reaches 2.65. When the expansion radius of the soil plastic zone $R_P$ is less than 2.65 times that of the slurry expansion radius $R_u$, the water pressure at the grouting outlet has a larger influence on the limit value of grouting pressure, especially when the expansion radius of the soil plastic zone is close to the slurry expansion radius; that is, when the expansion radius of the soil plastic zone is less than 1.5 times that of the slurry expansion radius. The water pressure at the grouting outlet is the dominant factor affecting the grouting pressure limit. Because the radius of the plastic zone is small at the beginning of slurry diffusion, the resistance pressure is mainly borne by the water pressure at the grouting outlet.

When $\beta_u$ is greater than 2.65, the effective internal friction angle of the loess stratum has a significant influence on the limiting value of grouting pressure. When $\beta_u$ is greater than 4, it can be considered that the effective internal friction angle of the stratum has a dominant influence on the limiting value of grouting pressure. When the radius of the plastic zone is large, the grouting pressure offsets the effect of the water pressure at the grouting outlet. At this time, the effective friction angle of the soil has
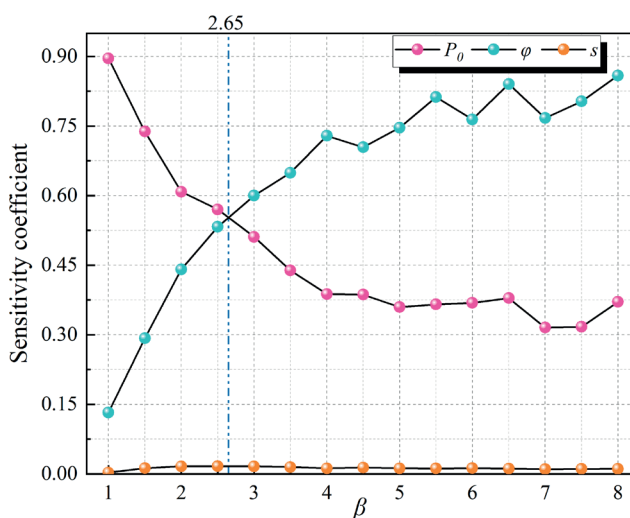


**Fig. 15** Factors influencing sensitivity on the upper limit of secondary grouting pressure

a significant influence on grout diffusion. Thus, the results of the sensitivity analysis are consistent with the practical engineering experience, which verifies the rationality of the theoretical analysis.

**5 Conclusions**
(1) Based on the unified strength criterion, a critical pressure calculation formula for secondary grouting in a loess stratum is proposed. The existing slurry diffusion model is appropriately simplified for the construction of backfill grouting. The critical pressure due to secondary grouting in the loess stratum was analyzed from an application perspective, and the critical grouting pressure corresponding to the supporting project was calculated to be 821.80 kPa.

(2) Based on the linear superposition principle of stress, the bolt stress under the gravity condition of the loess stratum obtained by Explicit analysis and the bolt stress under secondary grouting (821.80 kPa) simulated by the SPH theory are superimposed. The results showed that the maximum displacement of the segment related to grouting reached 3 cm before the bolt yields when the bolt stress was 560.50 MPa. The numerical simulation results verify that the theoretical analysis has certain reliability (the safety factor is 1.14).

(3) When the soil plastic zone expansion radius $R_P$ is less than 2.65 times that of the slurry expansion radius $R_u$, the water pressure at the grouting outlet has a significant influence on the critical grouting pressure limit; especially when the expansion radius of the soil plastic zone is less than 1.5 times the expansion radius of slurry, with the water pressure at the grouting outlet being the main influencing factor of the critical grouting pressure limit. When $\beta_u$ is greater than 2.65, the effective internal friction angle of the soil layer has a significant influence on the critical grouting pressure limit. When $\beta_u$ is greater than 4, the effective internal friction angle of the stratum is the main influencing factor of the critical grouting pressure limit. In actual analysis, the influence of matric suction on the critical grouting pressure limit can be ignored.

In addition, when the theoretical solution of the critical grouting pressure was obtained based on the condition of bolt shear failure, the deformation degree of the segments was not considered. The numerical simulation showed that the segment deformation was too large before bolt failure occurred. At this time, the bolt stress does not reach the yield state. The results showed that the critical grouting pressure obtained by theoretical analysis is relatively

conservative, which can guide secondary grouting construction of shield tunnels in loess strata. The results of the theoretical analysis and numerical simulation need to be further verified through field tests.

## References

[1] Kuang, G., Li, B., Mo, S., Hu, X., Li, L. "Review on Machine Learning-based Defect Detection of Shield Tunnel Lining", Periodica Polytechnica Civil Engineering, 66(3), pp. 943–957, 2022.
https://doi.org/10.3311/PPci.19859

[2] Zhang, T., Yang, P., Zhang, Y. "Investigation of Frost-Heaving Characteristics of Horizontal-Cup-Shape Frozen Ground Surface for Reinforced End Soil Mass in Shield Tunnel Construction", Periodica Polytechnica Civil Engineering, 61(3), pp. 541–547, 2017.
https://doi.org/10.3311/PPci.10169

[3] Rastbood, A., Gholipour, Y., Majdi, A. "Stress Analysis of Segmental Tunnel Lining Using Artificial Neural Network", Periodica Polytechnica Civil Engineering, 61(4), pp. 664–676, 2017.
https://doi.org/10.3311/PPci.9700

[4] Ye, F., Gou, C., Liu, Y., Sun, H. "Half-spherical surface diffusion model of shield tunnel back-filled grouts", Journal of Tong Ji University (Natural Science), 40, pp. 1789–1794, 2012. (in Chinese)

[5] Ye, F., Chen, Z., Gou, C., Mao, Y., Liu, Q. "Back-filled grouting compaction model of shield tunnel based on spherical cavity expansion", Journal of Traffic and Transportation Engineering, 14, pp. 35–42, 2014. (in Chinese)

[6] Qin, N., Ye, F., He, B., Liang, X., Han, X., Su, E. "Model study on backfill grouting in shield tunnels based on fractal theory", European Journal of Environmental and Civil Engineering, 2021.
https://doi.org/10.1080/19648189.2021.1925158

[7] Ye, F., Gou, C. F., Chen, Z., Liu, Y. P., Zhang, J. L. "Back-filled Grouts Diffusion Model of Shield Tunnel Considering Its Viscosity Degeneration", China Journal of Highway and Transport, 26, pp. 127–134, 2013. (in Chinese)
https://doi.org/10.19721/j.cnki.1001-7372.2013.01.018

[8] Gou, C. F., Ye, F., Zhang, J. L., Liu, Y. P. "Ring distribution model of filling pressure for shield tunnels under synchronous grouting", Chinese Journal of Geotechnical Engineering, 35, pp. 590–598, 2013. (in Chinese)

[9] Ye, F., Yang, T., Mao, J., Qin, X., Zhao, R. "Half-spherical surface diffusion model of shield tunnel back-fill grouting based on infiltration effect", Tunnelling and Underground Space Technology, 83, pp. 274–281, 2019.
https://doi.org/10.1016/j.tust.2018.10.004

[10] Liu, X.-X., Shen, S.-L., Xu, Y.-S., Zhou, A. "A diffusion model for backfill grout behind shield tunnel lining", International Journal for Numerical and Analytical Methods in Geomechanics, 45(4), pp. 457–477, 2021.
https://doi.org/10.1002/nag.3164

[11] Li, C. "Simplified algorithm for grouting pressure and grouting quantity in shield construction", International Journal of Civil Engineering, 18, pp. 419–428, 2020.
https://doi.org/10.1007/s40999-019-00476-5

[12] Liu, C., Li, J., Zhang, Z., Li, P., Cui, J., Liu, H., Yang, Y. "Model tests on tail-grouting process during URUP shield tunneling in soft soil", Tunnelling and Underground Space Technology, 103, 103451, 2020.
https://doi.org/10.1016/j.tust.2020.103451

[13] Mei, Y., Zhang, X., Nong, X., Fu, L. "Experimental study of the comprehensive technology of grouting and suspension under an operating railway in the cobble stratum", Transportation Geotechnics, 30, 100612, 2021.
https://doi.org/10.1016/j.trgeo.2021.100612

[14] Ding, Z., He, S.-Y., Zhou, W.-H., Xu, T., He, S.-H., Zhang, X. "Analysis of ground deformation induced by shield tunneling considering the effects of muck discharge and grouting", Transportation Geotechnics, 30, 100629, 2021.
https://doi.org/10.1016/j.trgeo.2021.100629

[15] Li, P., Liu, J., Shi, L., Li, X., Zhu, H., Huang, D., Kou, X. "Two-phase analytical model of seepage during grout consolidation around shield tunnel considering the temporal variation in viscosity and the infiltration effect", European Journal of Environmental and Civil Engineering, 2020.
https://doi.org/10.1080/19648189.2020.1852603

[16] Njock, P. G. A., Shen, S. "Investigation of ground displacement induced by hydraulic jetting using smoothed particle hydrodynamics", In: Proceedings of GeoShanghai 2018 International Conference: Ground Improvement and Geosynthetics, Shanghai, China, 2018, pp. 68–75. ISBN 978-981-13-0011-0.
https://doi.org/10.1007/978-981-13-0122-3_8

[17] Cao, G., Li, Z. "Numerical flow simulation of fresh concrete with viscous granular material model and smoothed particle hydrodynamics", Cement and Concrete Research, 100, pp. 263–274, 2017.
https://doi.org/10.1016/j.cemconres.2017.07.005

[18] Wu, H., Atangana Njock, P. G., Chen, J., Shen, S. "Numerical simulation of spudcan-soil interaction using an improved smoothed particle hydrodynamics (SPH)method", Marine Structures, 66, pp. 213–226, 2019.
https://doi.org/10.1016/j.marstruc.2019.04.007

[19] Li, P. N., Huang, D. Z., Zhu, Y. F., Ding, W. Q. "Diffusion mechanism and parameters acquisition of quasi-rectangular shield synchronous grouting using SPH method", Journal of Tong Ji University (Natural Science), 45, pp. 1592–1601, 2017. (in Chinese)

[20] Xiao, G. L., Li, P. N., Zhu, Y. F., Huang, D. Z., Zhu, H. H. "Explorative research on SPH fluid dynamics applied in quasi-rectangular shield construction", Modern Tunnelling Technology, 53, pp. 181–188, 2016.
https://doi.org/10.13807/j.cnki.mtt.2016.S1.026

[21] Li, P. N., Ding, W. Q., Huang, D. Z., Li, G. "Research on movement pattern of synchronous grouting in special-shaped s-hield using smoothed partide hydrodynamics simulation and test verification", Journal of Tong Ji University (Natural Science), 46, pp. 891–898, 2018. (in Chinese)

[22] Li, P., Liu, J., Zhai, Y., Ding, W., "Analysis and application exploration of smoothed particle hydrodynamics (SPH) for non-circular shield tunneling", In: Proceedings of GeoShanghai 2018 International Conference: Tunnelling and Underground Construction, Shanghai, China, 2018, pp. 432–441. ISBN 978-981-13-0011-0.
https://doi.org/10.1007/978-981-13-0017-2_43

[23] Pye, K. "Loess", Progress in Physical Geography: Earth and Environment, 8(2), pp. 176–217, 1984.
https://doi.org/10.1177/030913338400800202

[24] Zhang, C., Fan, W., Zhao, J. "Unified strength theory of unsaturated soils and verification with true triaxial test", Chinese Journal of Rock Mechanics and Engineering, 34, pp. 1702–1711, 2015. (in Chinese)
https://doi.org/10.13722/j.cnki.jrme.2014.1335

[25] Ye, F., Gou, C. F., Mao, J. H., Yang, P. B., Chen, Z., Jia, T. "Calculation of critical grouting pressure during shield tunneling in clay stratum and analysis of the influencing factors", Rock and Soil Mechanics, 36, pp. 937–945, 2015.
https://doi.org/10.16285/j.rsm.2015.04.004

[26] Yuan, Z. H., Ni, W. K., Liu, R., Li, H. H. "Study of shear strength of unsaturated and undisturbed loess based on suction stress", Journal of He Fei University of Technology, 38, pp. 648–653, 2015. (in Chinese)

[27] Bi, Y. Q., Zhang, M. S., Gu, T. F., Feng, L. "Soil-water characteristics and strength indexes of unsaturated loess", Journal of Disaster Prevention and Mitigation Engineering, 38, pp. 520–527, 2018.
https://doi.org/10.13409/j.cnki.jdpme.2018.03.016

[28] Wang, J. W. "Study on the soil water characteristic curve and strength characteristics of unsaturated loess in east Gansu Province", Master, Lanzhou University of Technology, 2017. (in Chinese)

[29] Song, T. T., Zhou, S. H., Xu, R. Z. "Mechanism and determination of parameters of synchronous grouting in shield tunnelling", Chinese Journal of Underground Space and Engineering, 41, pp. 130–133, 2008. (in Chinese)

[30] State Administration for Market Regulation "Mechanical properties of fasteners—Bolts, screws and studs GB/T 3098.1-2010", China Academy of Machinery Science and Technology, Beijing, China, 2010. (in Chinese)

[31] Monaghan, J. J. "Smoothed Particle Hydrodynamics", Annual Review of Astronomy and Astrophysics, 30, pp. 543–574, 1992.
https://doi.org/10.1146/annurev.aa.30.090192.002551

[32] Monaghan, J. J. "Smoothed particle hydrodynamics and its diverse applications", Annual Review of Fluid Mechanics, 44, pp. 323–346, 2011.
https://doi.org/10.1146/annurev-fluid-120710-101220

[33] Yan, Q., Zhang, C., Wu, W., Zhu, H., Yang, W. "3D Numerical Simulation of Shield Tunnel Subjected to Swelling Effect Considering the Nonlinearity of Joint Bending Stiffness", Periodica Polytechnica Civil Engineering, 63(3), pp. 751–762, 2019.
https://doi.org/10.3311/PPci.13996

[34] Mohtadinia, M., Ahmadi, M. H., Fasaghandis, M. M., Dibavar, B. H., Davarpanah, S. M. "Statistical and Numerical Study of Chipping and Cracking in Segmental Lining", Periodica Polytechnica Civil Engineering, 64(3), pp. 869–886, 2020.
https://doi.org/10.3311/PPci.16037

[35] Zhang, W., Zhang, Q., Cao, W. "Study on stress and deformation of bolt joints of shield tunnel under static and seismic action", KSCE Journal of Civil Engineering, 25, pp. 3146–3159, 2021.
https://doi.org/10.1007/s12205-021-1339-4

[36] Lu, G., Fall, M. "Coupled modelling of the behaviour of soft cementitious material exposed to underground mines blasting", In: 11th International Conference on Shock & Impact Loads on Structures, Ottawa, Canada, 2015, pp. 1–9. ISBN 9810946376

[37] Ministry of Housing and Urban-Rural Development of the People's Republic of China "Code for construction and acceptance of shield tunnelling method GB 50446-2017", Center of Science and Technology & Industrialization Development, Beijing, China, 2017. (in Chinese)

[38] Zhang, Q., Du, S., Lu, M. "Research on Dislocation Monitoring for Shield Tunnel Segments with Straight Joint", Chinese Journal of Underground Space and Engineering, 41, pp. 138–142, 2008. (in Chinese)

[39] Liu, W., Ding, L. "Global sensitivity analysis of influential parameters for excavation stability of metro tunnel", Automation in Construction, 113, 103080, 2020.
https://doi.org/10.1016/j.autcon.2020.103080